Crystal structure, Hirshfeld surface analysis, calculations of crystal voids, interaction energy and energy frameworks as well as density functional theory (DFT) calculations of 3-[2-(morpholin-4-yl)-ethyl]-5,5-diphenylimidazolidine-2,4-dione

Houda Lamssane,[a]* Amal Haoudi,[a] Badr Eddine Kartah,[b] Ahmed Mazzah,[c] Joel T. Mague,[d] Tuncer Hökelek,[e] Youssef Kandri Rodi[a] and Nada Kheira Sebbar[f,b]

[a]Laboratory of Applied Organic Chemistry, Sidi Mohamed Ben Abdellah University, Faculty Of Science And Technology, Road Immouzer, BP 2202 Fez, Morocco, [b]Laboratory of Plant Chemistry, Organic and Bioorganic Synthesis, Faculty of Sciences, Mohammed V University in Rabat, 4 Avenue Ibn Battouta BP 1014 RP, Morocco, [c]Science and Technology of Lille USR 3290, Villeneuve d'ascq cedex, France, [d]Department of Chemistry, Tulane University, New Orleans, LA 70118, USA, [e]Department of Physics, Hacettepe University, 06800 Beytepe, Ankara, Türkiye, and [f]Laboratory of Organic and Physical Chemistry, Applied Bioorganic Chemistry Team, Faculty of Sciences, Ibnou Zohr University, Agadir, Morocco. *Correspondence e-mail: houda.lamssane@usmba.ac.ma

In the title molecule, $C_{21}H_{23}N_3O_3$, the imidazolidine ring slightly deviates from planarity and the morpholine ring exhibits the chair conformation. In the crystal, N—H···O and C—H···O hydrogen bonds form helical chains of molecules extending parallel to the c axis that are connected by C—H···π(ring) interactions. A Hirshfeld surface analysis reveals that the most important contributions for the crystal packing are from H···H (55.2%), H···C/C···H (22.6%) and H···O/O···H (20.5%) interactions. The volume of the crystal voids and the percentage of free space were calculated to be 236.78 $Å^3$ and 12.71%, respectively. Evaluation of the electrostatic, dispersion and total energy frameworks indicates that the stabilization is dominated by the nearly equal electrostatic and dispersion energy contributions. The DFT-optimized molecular structure at the B3LYP/6-311 G(d,p) level is compared with the experimentally determined molecular structure in the solid state. Moreover, the HOMO–LUMO behaviour was elucidated to determine the energy gap.

1. Chemical context

The investigation of compounds comprising the hydantoin moiety has gained interest in the quest for the development of new drugs because of their similarity to natural amino acids (Śladowska *et al.*, 2016). Such compounds show various pharmacological properties, including antibacterial (Pandeya *et al.*, 2000; Sangeetha *et al.*, 2016), anticonvulsant (Emami *et al.*, 2021), antidiabetic (Salem *et al.*, 2018), antitumor (Żesławska *et al.*, 2021), antinociceptive and anti-inflammatory (Abdel-Aziz *et al.*, 2016; da Silva Guerra *et al.*, 2011) activities. One of the foremost pharmaceutical drugs in the hydantoin class is phenytoin, also known as 5,5-diphenyl-hydantoin (systematic name: 5,5-diphenylimidazolidine-2,4-dione). This compound and its derivatives are considered to be potential pharmaceutical agents due to their extended shelf life. However, their optimum efficacy depends on how easily they break down in the body (Al-Nuzal *et al.*, 2018). With respect to the biological importance of phenytoin, we were interested in the synthesis of a new derivative thereof, *viz.* 3-[2-(morpholin-4-yl)ethyl]-5,5-diphenylimidazolidine-2,4-di-one, (**I**), $C_{21}H_{23}N_3O_3$, through an alkylation reaction under
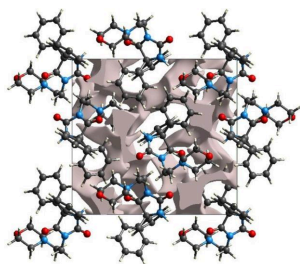
the conditions of phase transfer catalysis. We report here the molecular and crystal structures as well as the Hirshfeld surface analysis of this compound, as well as intermolecular interaction energies, energy frameworks, and a comparison of the experimentally determined molecular structure in the solid state with that of an optimized structure obtained by density functional theory (DFT).
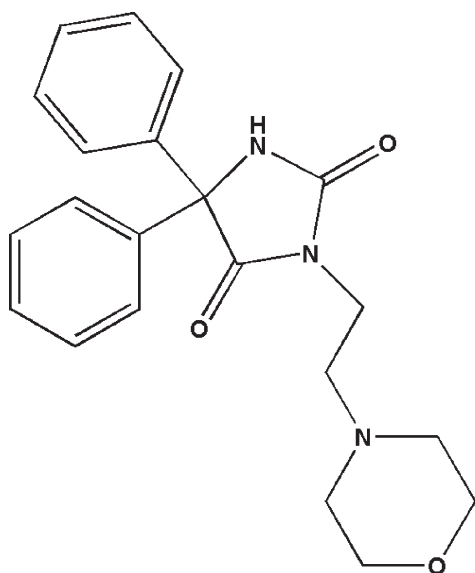
2. Structural commentary

The molecular structure of (**I**) is displayed in Fig. 1. The imidazolidine ring deviates from planarity (root-mean-square deviation of the fitted atoms = 0.0273 Å) with atoms C1 and N2 being displaced by 0.0359 (7) and −0.0359 (7) Å, respectively, from the mean plane. The C4–C9 and C10–C15 benzene rings are inclined to the above plane by 76.55 (4) and 65.07 (4)°, respectively. The N1—C2, N1—C3 and N2—C3 distances are 1.367 (2), 1.406 (2) and 1.348 (2) Å. The sums of the bond angles about N1 and N2 of 360.0 and 359° indicate that the lone electron pairs at the nitrogen atoms are involved
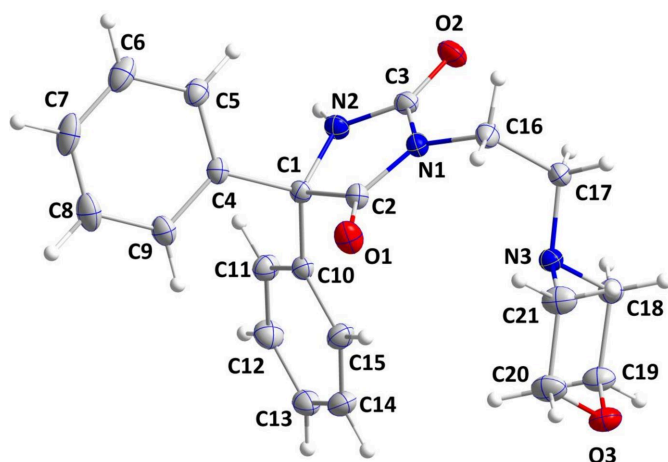
Table 1
Hydrogen-bond geometry (Å, °).

$Cg3$ is the centroid of the C4–C9 benzene ring.

D—H$\cdots A$	D—H	H$\cdots A$	$D\cdots A$	D—H$\cdots A$
N2—H2$\cdots$O3^i	0.91 (1)	1.95 (1)	2.8560 (15)	179 (2)
C12—H12$\cdots Cg3^{ii}$	0.95	2.62	3.5576 (15)	169
C18—H18$B\cdots Cg3^{iii}$	0.99	2.65	3.5726 (14)	155

Symmetry codes: (i) $-x + \frac{3}{2}, -y + 1, z + \frac{1}{2}$; (ii) $-x, y + \frac{3}{2}, -z + \frac{3}{2}$; (iii) $x + 1, y, z$.

in N→C π bonding. The morpholine ring adopts a chair conformation [puckering parameters (Cremer & Pople, 1975): Q = 0.5831 (14) Å, θ = 176.90 (14)°, φ = 339 (3)°].

3. Supramolecular features

In the crystal of (**I**), N2—H2$\cdots$O1 and C14—H14$\cdots$O2 hydrogen bonds (Table 1) form helical chains of molecules extending parallel to the c axis (Fig. 2). Individual molecules are connected by weak C12—H12$\cdots Cg3$ and C18—H18$B\cdots Cg3$ interactions (Table 1) into a tri-periodic network (Fig. 3), which appears to have small pores in
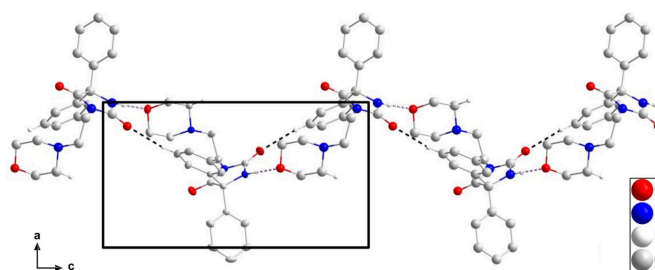
Figure 2
A portion of one helical chain in the crystal structure viewed along the b axis. N—H$\cdots$O and C—H$\cdots$O hydrogen bonds are depicted by violet and black dashed lines, respectively. Non-interacting hydrogen atoms are omitted for clarity.
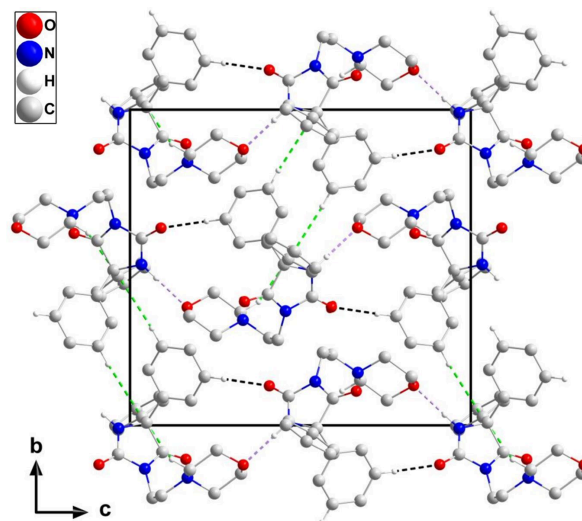
Figure 3
The crystal packing viewed along the a axis with N—H$\cdots$O and C—H$\cdots$O hydrogen bonds depicted by violet and black dashed lines, respectively, and with C—H$\cdots\pi$(ring) interactions depicted by green dashed lines. Non-interacting hydrogen atoms are omitted for clarity.

Figure 1
The title molecule with the labelling scheme and displacement ellipsoids drawn at the 50% probability level.

Figure 4
View of the three-dimensional Hirshfeld surface of (**I**) plotted over d_{norm}.

Figure 6
Hirshfeld surface of the title compound plotted over shape-index.

agreement with the calculation of a relatively small void space (*vide infra*).

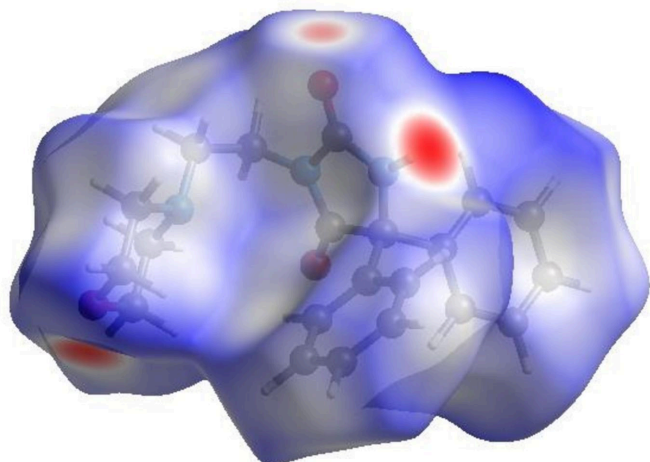## 4. Hirshfeld surface analysis

In order to visualize the intermolecular interactions in the crystal of (**I**), a Hirshfeld surface (HS) analysis (Hirshfeld, 1977; Spackman & Jayatilaka, 2009) was carried out using *CrystalExplorer* (Spackman *et al.*, 2021). In the HS plotted over d_{norm} (Fig. 4), the white surface indicates contacts with distances equal to the sum of van der Waals radii and the red and blue colours indicate distances shorter (in close contact) or longer (distant contact) than the sum of the van der Waals radii, respectively (Venkatesan *et al.*, 2016). The bright-red spots on the surface indicate the roles of adjacent atoms as the respective donors and/or acceptors and they also appear as
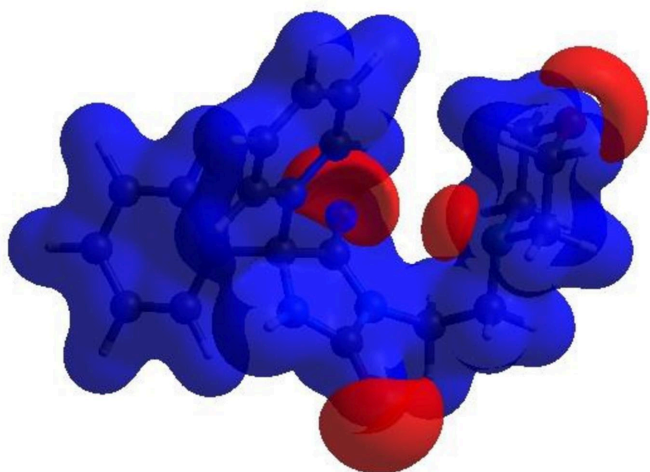
blue and red regions corresponding to positive (hydrogen-bond donors) and negative (hydrogen-bond acceptors) potentials on the HS mapped over electrostatic potential (Spackman *et al.*, 2008; Jayatilaka *et al.*, 2005), as shown in Fig. 5. The shape-index of the HS is a tool to visualize π–π stacking by the presence of adjacent red and blue triangles. However, Fig. 6 clearly suggests that there are no π–π interactions in the crystal structure of (**I**). The overall two-dimensional fingerprint plot, Fig. 7a, and those delineated into H$\cdots$H, H$\cdots$C/C$\cdots$H, H$\cdots$O/O$\cdots$H and H$\cdots$N/N$\cdots$H (McKinnon *et al.*, 2007) are illustrated in Fig. 7b–e, respectively, together with their relative contributions to the Hirshfeld surface. The most abundant interaction is H$\cdots$H, contributing with 55.2% to the overall crystal packing, which is reflected in Fig. 7b as widely scattered points of high density due to the large hydrogen content with the tip at $d_e = d_i = 1.10$ Å. The H$\cdots$C/C$\cdots$H contacts, contributing with 22.6% to

Figure 5
View of the three-dimensional Hirshfeld surface of (**I**) plotted over electrostatic potential energy using the STO-3 G basis set at the Hartree–Fock level of theory. Hydrogen-bond donors and acceptors are shown as blue and red regions around the atoms corresponding to positive and negative potentials, respectively.
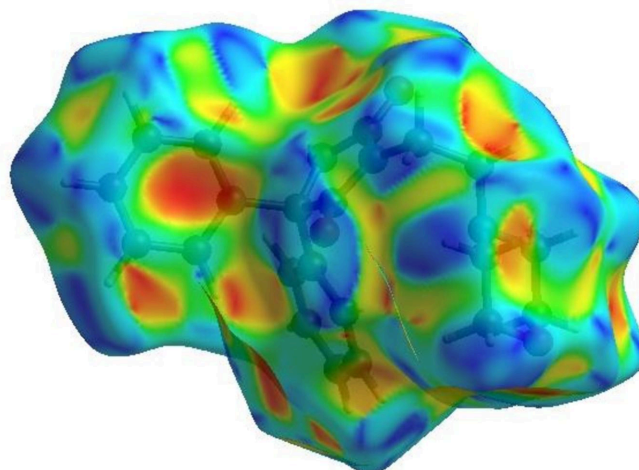

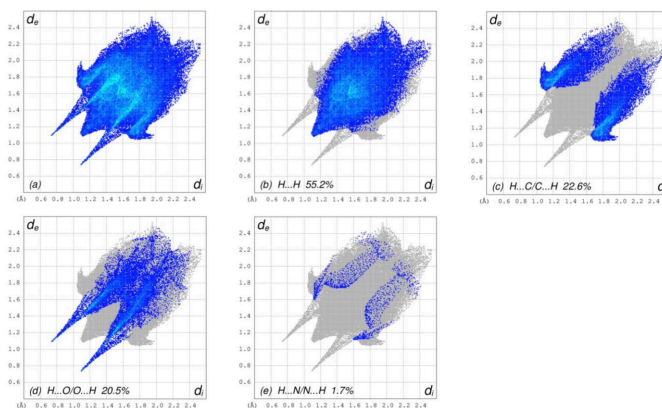**Figure 7**
The full two-dimensional fingerprint plots for (**I**), showing (a) all interactions, and delineated into (b) H$\cdots$H, (c) H$\cdots$C/C$\cdots$H, (d) H$\cdots$O/O$\cdots$H and (e) H$\cdots$N/N$\cdots$H interactions. The d_i and d_e values are the closest internal and external distances (in Å) from given points on the Hirshfeld surface.
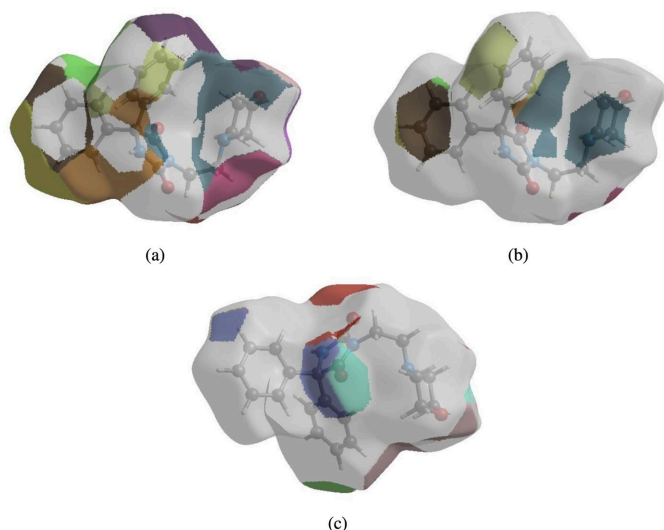
Figure 8
Hirshfeld surface patches plotted onto the surface for (*a*) H···H, (*b*) H···C/C···H and (*c*) H···O/O···H interactions.

the overall crystal packing, are shown in Fig. 7*c* with the tips at $d_e + d_i = 2.74$ Å and are attributed to C—H···π interactions. The symmetrical pair of spikes in the fingerprint plot delineated into H···O/O···H contacts with the tips at $d_e + d_i = 1.84$ Å (Fig. 7*d*) make a 20.5% contribution to the HS. Finally, the tiny pair of spikes with the tips at $d_e + d_i = 2.70$ Å in the fingerprint plot delineated into H···N/N···H contacts (Fig. 7*e*) contributes only 1.7% to the HS.

The nearest neighbour coordination environment of a molecule can be determined from the colour patches on the HS based on how close to other molecules they are. The Hirshfeld surface representations with the function d_{norm} plotted onto the surface are shown for the H···H, H···C/ C···H and H···O/O···H interactions in Fig. 8*a–c*. The Hirshfeld surface analysis confirms the importance of H-atom contacts in establishing the packing. The large number of H···H, H···C/C···H and H···O/O···H interactions suggest that van der Waals interactions and hydrogen-bonding interactions play the major roles in the crystal packing (Hathwar *et al.*, 2015).

5. Crystal voids

The strength of the crystal packing is important for determining the response to an applied mechanical force. If significant voids are present in the crystal, the molecules are not tightly packed and a small amount of applied external mechanical force may easily break the crystal. To check the mechanical stability of the crystal, a void analysis was performed by adding up the electron densities of the spherically symmetric atoms contained in the asymmetric unit (Turner *et al.*, 2011). The void surface is defined as an isosurface of the procrystal electron density and is calculated for the whole unit cell where the void surface meets the boundary of the unit cell, and capping faces are generated to create an enclosed volume. The volume of the crystal voids (Fig. 9*a,b*) and the percentage of free space in the unit cell were calculated as 236.78 Å^3 and 12.71%.

6. Interaction energy calculations and energy frameworks

The intermolecular interaction energies were calculated using the CE–B3LYP/6–31G(d,p) energy model available in *CrystalExplorer* (Spackman *et al.*, 2021) where a cluster of molecules is generated by applying crystallographic symmetry operations with respect to a selected central molecule within a radius of 3.8 Å (Turner *et al.*, 2014). The total intermolecular energy (E_{tot}) is the sum of electrostatic (E_{ele}), polarization (E_{pol}), dispersion (E_{dis}) and exchange-repulsion (E_{rep}) energies (Turner *et al.*, 2015) with scale factors of 1.057, 0.740, 0.871 and 0.618, respectively (Mackenzie *et al.*, 2017). Hydrogen-bonding interaction energies (in kJ mol^{-1}) were calculated to
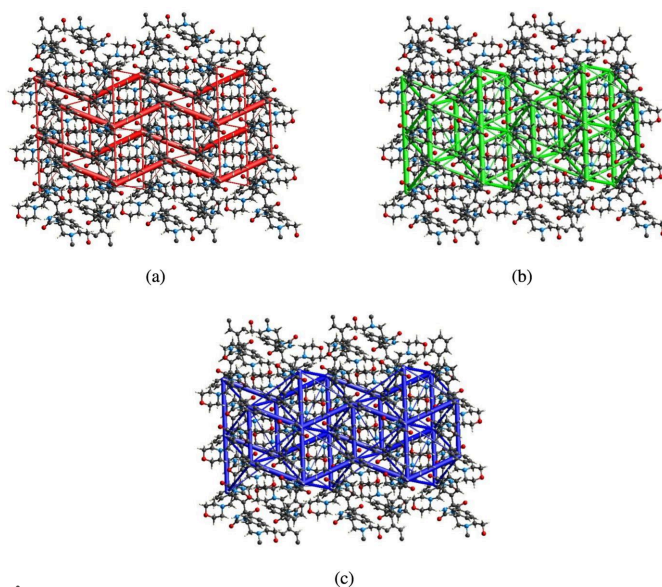
Figure 10
The energy frameworks for a cluster of molecules of (**I**) viewed down the *b* axis, showing (*a*) electrostatic energy, (*b*) dispersion energy and (*c*) total energy diagrams. The cylindrical radius is proportional to the relative strength of the corresponding energies and they were adjusted to the same scale factor of 80 with cut-off value of 5 kJ mol-1 within 2×2×2 unit cells.

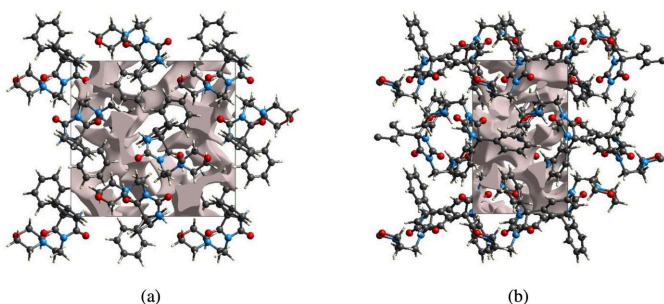**Figure 9**
Graphical views of voids in the crystal packing of (**I**), (*a*) along the *a* axis and (*b*) along the *c* axis.

Table 2
Comparison of the selected (X-ray and DFT) geometric data (Å, °).

Bonds/angles	X-ray	B3LYP/6–311G(d,p)
O1—C2	1.2105 (15)	1.221
O2—C3	1.2183 (15)	1.223
O3—C20	1.4306 (19)	1.445
N1—C2	1.3670 (16)	1.357
N1—C3	1.4058 (16)	1.420
N2—C3	1.3485 (16)	1.338
N2—H2	0.910 (12)	0.920
N3—C17	1.4568 (16)	1.464
C20—O3—C19	110.21 (11)	111.25
C3—N2—C1	113.03 (10)	114.18
N2—C1—C4	112.19 (9)	112.69
N2—C1—C10	110.29 (9)	110.87
N2—C1—C2	100.70 (9)	100.98
O1—C2—N1	126.69 (12)	125.98
O2—C3—N2	128.46 (13)	128.52
O2—C3—N1	124.27 (12)	124.75
N2—C3—N1	107.27 (10)	107.64

Table 3
Calculated energies.

Molecular Energy (a.u.) (eV)	Compound (**I**)
Total Energy, TE (eV)	–32761.48
E_{HOMO} (eV)	–5.36
E_{LUMO} (eV)	–0.73
Gap, ΔE (eV)	4.62
Dipole moment, μ (Debye)	2.406
Ionization potential, I (eV)	–5.36
Electron affinity, A	–0.73
Electro negativity, χ	–3.04
Hardness, η	–2.31
Electrophilicity index, ω	–2.00
Softness, σ	0.35
Fraction of electrons transferred, ΔN	–2.17

be $-50.2(E_{ele})$, -12.7 (E_{pol}), -27.6 (E_{dis}), 58.2 (E_{rep}) and -50.5 (E_{tot}) for N2—H2···O3 and -17.4 (E_{ele}), -3.7 (E_{pol}), -56.2 (E_{dis}), 43.2 (E_{rep}) and -43.4 (E_{tot})] for C14—H14···O2. Energy frameworks combine the calculation of intermolecular interaction energies with a graphical representation of their magnitude (Turner *et al.*, 2015). Energies between molecular pairs are represented as cylinders joining the centroids of pairs of molecules with the cylinder radius proportional to the relative strength of the corresponding interaction energy. Energy frameworks were constructed for E_{ele} (red cylinders), E_{dis} (green cylinders) and E_{tot} (blue cylinders) and are displayed in Fig. 10*a–c*. The evaluation of the electrostatic, dispersion and total energy frameworks indicate that the stabilization is dominated by nearly equal electrostatic and dispersion energy contributions in the crystal structure of (**I**).

7. DFT calculations

The optimization of the molecular gas-phase structure of (**I**) was conducted using density functional theory (DFT) with the B3LYP functional and 6-311G(d,p) basis-set calculations, as implemented in *GAUSSIAN09* (Becke, 1993; Frisch *et al.*, 2009). The comparison between theoretical and experimental results revealed good agreement (Table 2). Essential parameters, such as the highest-occupied molecular orbital (HOMO) serving as an electron donor and the lowest-unoccupied molecular orbital (LUMO) acting as an electron acceptor, were examined, whereby a small energy gap indicates high molecular polarizability and reactivity. Numerical parameters of E_{HOMO}, E_{LUMO}, electronegativity (χ), hardness (η), potential (μ), electrophilicity (ω), and softness (σ) are detailed in Table 3. The values of χ and η are particularly significant for assessing both reactivity and stability. The electron transition from the HOMO to the LUMO energy level is shown in Fig. 11. Both the HOMO and LUMO are localized in the molecular plane. The energy band gap ($E = E_{LUMO} - E_{HOMO}$) is approximately 4.62 eV, with frontier molecular orbital (FMO) energies, E_{HOMO} and E_{LUMO}, determined as -5.36 and -0.73 eV, respectively.

8. Database survey

A search of the Cambridge Structural Database (CSD; Groom *et al.*, 2016; updated January 2024) with the fragment (**II**) (Fig. 12) gave ten hits, one of which (LUHFID; Ooms *et al.*,

E_{LUMO} = -0.73 eV

ΔE = 4.62 eV

E_{HOMO} = -5.36 eV

Figure 11
The energy band gap of the title compound.

II

Figure 12
The molecular moiety used for the CSD search procedure.

2002) is the same as (**I**) except for having a bromine atom at the 4-position of each phenyl ring. Here, the C—N distances in the ring are similar, indicating delocalization of the π elect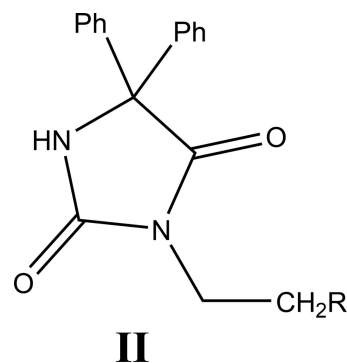rons. Although the morpholine ring also adopts a chair conformation, the large displacement ellipsoids for the constituent atoms indicate at least considerable librational motion and likely some degree of positional disorder. The remaining matches have R = H (FEHPUG; Guerrab *et al.*, 2017*a*), Me (WEMQUD; Guerrab *et al.*, 2017*c* and WEMQUD01; Trišovic *et al.*, 2019), Et (QENBET; Guerrab *et al.*, 2018*a*), –(CH$_2$)$_2$Me (GEMSOG; Guerrab *et al.*, 2017*b*), –(CH$_2$)$_3$Me (QENBOD; Guerrab *et al.*, 2018*b*), –(CH$_2$)$_5$Me (QAGPAT; Guerrab *et al.*, 2020), –(CH$_2$)$_7$Me (PAJMAS; Guerrab *et al.*, 2022) and Br (NIBMOE; Guerrab *et al.*, 2023). In all cases, the five-membered ring is close to planarity and the nitrogen lone pairs are involved in N→C π bonding.

9. Synthesis and crystallization

In a flask, phenytoin (0.5 g, 1.98 mmol) was mixed with 4-(2-chloroethyl)morpholine hydrochloride (0.37 g, 1.01 mmol) in DMF (20 ml) in the presence of potassium carbonate (0.41 g, 2.96 mmol) and tetra-*n*-butylammonium bromide (BTBA, 0.07 g, 0.22 mmol). The reaction mixture was agitated for 48 h at room temperature, followed by removal of the solvent under reduced pressure. The residue was purified by recrystallization from methanol. Yield: 85%, R_f: 0.17 (ethyl acetate/hexane: 1/2), m.p. 363 K, LCMS (ESI): 366.1812 [M+H$^+$], ^{1}H NMR (CDCl$_3$-300 MHz): δ (ppm) 7.36–7.47 (*m*, 10H, H$_{Ar}$); 7.08 (*s*, 1H, NH), 3.72 (*t*, 2H, CH$_2$, $^3J_{H–H}$ = 6 MHz), 3.60 (*t*, 4H, CH$_2$, $^3J_{H–H}$ = 6 MHz), 2.65 (*t*, 2H, CH$_2$, $^3J_{H–H}$ = 6 MHz), 2.50 (*t*, 4H, CH$_2$, $^3J_{H–H}$ = 6 MHz), ^{13}C NMR (CDCl$_3$ −75 MHz): δ (ppm) 173.71, 156.65 (C=O); 139.26, 70.19 (Cq); 126.88-128.80 (CH$_{Ar}$); 66.83, 55.26, 53.32, 35.66 (CH$_2$). UV–Visible Wavelength (nm) λ$_{max}$: 286 in dichloromethane.

10. Refinement

Crystal data, data collection and structure refinement details are summarized in Table 4. H atoms attached to C atoms were placed in calculated positions (C—H = 0.95–0.99 Å) and were included as riding contributions with isotropic displacement parameters 1.2–1.5 times those of the attached atoms. The H atom attached to N2 was found in a difference-Fourier map and refined with a distance of 0.91 (1) Å. Two reflections, 111 and 011, affected by the beamstop were omitted from the final refinement.

Funding information

Table 4
Experimental details.

Crystal data	
Chemical formula	C$_{21}$H$_{23}$N$_3$O$_3$
M_r	365.42
Crystal system, space group	Orthorhombic, $P2_12_12_1$
Temperature (K)	150
a, b, c (Å)	8.4440 (3), 14.3013 (5), 15.4233 (6)
V (Å^3)	1862.52 (12)
Z	4
Radiation type	Mo $K\alpha$
μ (mm^{-1})	0.09
Crystal size (mm)	0.28 × 0.18 × 0.17
Data collection	
Diffractometer	Bruker D8 QUEST PHOTON 3 diffractometer
Absorption correction	Numerical (*SADABS*; Krause *et al.*, 2015)
T_{min}, T_{max}	0.98, 0.98
No. of measured, independent and observed [$I > 2\sigma(I)$] reflections	142315, 7105, 6502
R_{int}	0.052
$(\sin \theta/\lambda)_{max}$ (Å^{-1})	0.771
Refinement	
$R[F^2 > 2\sigma(F^2)]$, $wR(F^2)$, S	0.037, 0.097, 1.07
No. of reflections	7105
No. of parameters	247
No. of restraints	1
H-atom treatment	H atoms treated by a mixture of independent and constrained refinement
$\Delta\rho_{max}, \Delta\rho_{min}$ (e Å^{-3})	0.29, −0.19
Absolute structure	Flack x determined using 2747 quotients [$(I^+)-(I^-)$]/[$(I^+)+(I^-)$] (Parsons *et al.*, 2013)
Absolute structure parameter	0.12 (18)

Computer programs: *APEX4* and *SAINT* (Bruker, 2021), *SHELXT* (Sheldrick, 2015*a*), *SHELXL* (Sheldrick, 2015*b*), *DIAMOND* (Brandenburg & Putz, 2012), *SHELXTL* (Sheldrick, 2008) and *PLATON* (Spek, 2020).

References

Abdel-Aziz, A. A. M., El-Azab, A. S., Abou-Zeid, L. A., ElTahir, K. E. H., Abdel-Aziz, N. I., Ayyad, R. R. & Al-Obaid, A. M. (2016). *Eur. J. Med. Chem.* **115**, 121–131.

Al-Nuzal, S. M. D., Al-Dulaimi, M. F. & Hassan, A. T. (2018). *J. Univ. Anbar Pure Sci.*, **12**, 38–53. https://doi.org/10.37652/juaps.2022.17150

Akrad, R., Guerrab, W., Lazrak, F., Ansar, M., Taoufik, J., Mague, J. T. & Ramli, Y. (2018*a*). *IUCrData*, **3**, x180934.

Becke, A. D. (1993). *J. Chem. Phys.* **98**, 5648–5652.

Brandenburg, K. & Putz, H. (2012). *DIAMOND*, Crystal Impact GbR, Bonn, Germany.

Bruker (2021). *APEX4* and *SAINT*. Bruker AXS LLC, Madison, Wisconsin, USA.

Cremer, D. & Pople, J. A. (1975). *J. Am. Chem. Soc.* **97**, 1354–1358.

Emami, S., Valipour, M., Kazemi Komishani, F., Sadati-Ashrafi, F., Rasoulian, M., Ghasemian, M., Tajbakhsh, M., Honarchian Masihi, P., Shakiba, A., Irannejad, H. & Ahangar, N. (2021). *Bioorg. Chem.* **112**, 104943.

Frisch, M. J., Trucks, G. W., Schlegel, H. B., Scuseria, G. E., Robb, M. A., Cheeseman, J. R., Scalmani, G., Barone, V., Mennucci, B., Petersson, G. A., Nakatsuji, H., Caricato, M., Li, X., Hratchian, H. P., Izmaylov, A. F., Bloino, J., Zheng, G., Sonnenberg, J. L., Hada, M., Ehara, M., Toyota, K., Fukuda, R., Hasegawa, J., Ishida, M., Nakajima, T., Honda, Y., Kitao, O., Nakai, H., Vreven, T., Montgomery, J. A. Jr, Peralta, J. E., Ogliaro, F., Bearpark, M., Heyd, J. J., Brothers, E., Kudin, K. N., Staroverov, V. N., Kobayashi, R., Normand, J., Raghavachari, K., Rendell, A., Burant, J. C., Iyengar,

S. S., Tomasi, J., Cossi, M., Rega, N., Millam, J. M., Klene, M., Knox, J. E., Cross, J. B., Bakken, V., Adamo, C., Jaramillo, J., Gomperts, R., Stratmann, R. E., Yazyev, O., Austin, A. J., Cammi, R., Pomelli, C., Ochterski, J. W., Martin, R. L., Morokuma, K., Zakrzewski, V. G., Voth, G. A., Salvador, P., Dannenberg, J. J., Dapprich, S., Daniels, A. D., Farkas, O., Foresman, J. B., Ortiz, J. V., Cioslowski, J. & Fox, D. J. (2009). *GAUSSIAN09*. Gaussian Inc., Wallingford, CT, USA.

Groom, C. R., Bruno, I. J., Lightfoot, M. P. & Ward, S. C. (2016). *Acta Cryst.* B**72**, 171–179.

Guerrab, W., Akrad, R., Ansar, M., Taoufik, J., Mague, J. T. & Ramli, Y. (2017*a*). *IUCrData*, **2**, x171591.

Guerrab, W., Akrad, R., Ansar, M., Taoufik, J., Mague, J. T. & Ramli, Y. (2017*b*). *IUCrData*, **2**, x171693.

Guerrab, W., El Jemli, M., Akachar, J., Demirtaş, G., Mague, J. T., Taoufik, J., Ibrahimi, A., Ansar, M., Alaoui, K. & Ramli, Y. (2022). *J. Biomol. Struct. Dynam.* **40**, 8765–8782.

Guerrab, W., El Moutaouakil Ala Allah, A., Alsubari, A., Mague, J. T. & Ramli, Y. (2023). *IUCrData*, **8**, x230060.

Guerrab, W., Mague, J. T. & Ramli, Y. (2020). *Z. Krist. New Cryst. Struct.* **235**, 1425–1427.

Guerrab, W., Mague, J. T., Taoufik, J. & Ramli, Y. (2018*b*). *IUCrData*, **3**, x180057.

Guerrab, W., Mague, J. T., Akrad, R., Ansar, M., Taoufik, J. & Ramli, Y. (2017*c*). *IUCrData*, **2**, x171808.

Hathwar, V. R., Sist, M., Jørgensen, M. R. V., Mamakhel, A. H., Wang, X., Hoffmann, C. M., Sugimoto, K., Overgaard, J. & Iversen, B. B. (2015). *IUCrJ*, **2**, 563–574.

Hirshfeld, H. L. (1977). *Theor. Chim. Acta*, **44**, 129–138.

Jayatilaka, D., Grimwood, D. J., Lee, A., Lemay, A., Russel, A. J., Taylor, C., Wolff, S. K., Cassam-Chenai, P. & Whitton, A. (2005). *TONTO* - A System for Computational Chemistry. Available at: http://hirshfeldsurface.net/

Krause, L., Herbst-Irmer, R., Sheldrick, G. M. & Stalke, D. (2015). *J. Appl. Cryst.* **48**, 3–10.

Mackenzie, C. F., Spackman, P. R., Jayatilaka, D. & Spackman, M. A. (2017). *IUCrJ*, **4**, 575–587.

McKinnon, J. J., Jayatilaka, D. & Spackman, M. A. (2007). *Chem. Commun.* pp. 3814.

Ooms, F., Wouters, J., Oscari, O., Happaerts, T., Bouchard, G., Carrupt, P.-A., Testa, B. & Lambert, D. M. (2002). *J. Med. Chem.* **45**, 1748–1756.

Pandeya, S. N., Sriram, D., Nath, G. & De Clercq, E. (2000). *Eur. J. Med. Chem.* **35**, 249–255.

Parsons, S., Flack, H. D. & Wagner, T. (2013). *Acta Cryst.* B**69**, 249–259.

Salem, M. G., Abdel Aziz, Y. M., Elewa, M., Elshihawy, H. A. & Said, M. M. (2018). *Bioorg. Chem.* **79**, 131–144.

Sangeetha, P., Siva, T., Balaji, R., & Tharini2, and K. (2016). *World J. Sci. and Res.* **1**, 26–30.

Sheldrick, G. M. (2008). *Acta Cryst.* A**64**, 112–122.

Sheldrick, G. M. (2015*a*). *Acta Cryst.* A**71**, 3–8.

Sheldrick, G. M. (2015*b*). *Acta Cryst.* C**71**, 3–8.

Silva Guerra, A. S. H. da, do Nascimento Malta, D. J., Morais Laranjeira, L. P., Souza Maia, M. B., Cavalcanti Colaço, N., do Carmo Alves de Lima, M., Galdino, S. L., da Rocha Pitta, I. & Gonçalves-Silva, T. (2011). *Int. Immunopharmacol.* **11**, 1816–1822.

Śladowska, K., Handzlik, J., Kieć-Kononowicz, K. & Mazur, L. (2016). *Indian J. Exp. Biol.* **54**, 553–559.

Spackman, M. A. & Jayatilaka, D. (2009). *CrystEngComm*, **11**, 19–32.

Spackman, M. A., McKinnon, J. J. & Jayatilaka, D. (2008). *CrystEngComm*, **10**, 377–388.

Spackman, P. R., Turner, M. J., McKinnon, J. J., Wolff, S. K., Grimwood, D. J., Jayatilaka, D. & Spackman, M. A. (2021). *J. Appl. Cryst.* **54**, 1006–1011.

Spek, A. L. (2020). *Acta Cryst.* E**76**, 1–11.

Trišović, N., Radovanović, L., Janjić, G. V., Jelić, S. T. & Rogan, J. (2019). *Cryst. Growth Des.* **19**, 2163–2174.

Turner, M. J., Grabowsky, S., Jayatilaka, D. & Spackman, M. A. (2014). *J. Phys. Chem. Lett.* **5**, 4249–4255.

Turner, M. J., McKinnon, J. J., Jayatilaka, D. & Spackman, M. A. (2011). *CrystEngComm*, **13**, 1804–1813.

Turner, M. J., Thomas, S. P., Shi, M. W., Jayatilaka, D. & Spackman, M. A. (2015). *Chem. Commun.* **51**, 3735–3738.

Venkatesan, P., Thamotharan, S., Ilangovan, A., Liang, H. & Sundius, T. (2016). *Spectrochim. Acta A Mol. Biomol. Spectrosc.* **153**, 625–636.

Żesławska, E., Kucwaj-Brysz, K., Kincses, A., Spengler, G., Szymańska, E., Czopek, A., Marć, M. A., Kaczor, A., Nitek, W., Domínguez-Álvarez, E., Latacz, G., Kieć-Kononowicz, K. & Handzlik, J. (2021). *Bioorg. Chem.* **109**, 104735.

supporting information

Crystal structure, Hirshfeld surface analysis, calculations of crystal voids, interaction energy and energy frameworks as well as density functional theory (DFT) calculations of 3-[2-(morpholin-4-yl)ethyl]-5,5-diphenyl-imidazolidine-2,4-dione

Houda Lamssane, Amal Haoudi, Badr Eddine Kartah, Ahmed Mazzah, Joel T. Mague, Tuncer Hökelek, Youssef Kandri Rodi and Nada Kheira Sebbar

Computing details

3-[2-(Morpholin-4-yl)ethyl]-5,5-diphenylimidazolidine-2,4-dione

Crystal data

$C_{21}H_{23}N_3O_3$	$D_x = 1.303$ Mg m^{-3}
$M_r = 365.42$	Mo $K\alpha$ radiation, $\lambda = 0.71073$ Å
Orthorhombic, $P2_12_12_1$	Cell parameters from 9478 reflections
$a = 8.4440$ (3) Å	$\theta = 2.8$–33.0°
$b = 14.3013$ (5) Å	$\mu = 0.09$ mm^{-1}
$c = 15.4233$ (6) Å	$T = 150$ K
$V = 1862.52$ (12) Å^3	Block, colourless
$Z = 4$	$0.28 \times 0.18 \times 0.17$ mm
$F(000) = 776$	

Data collection

Bruker D8 QUEST PHOTON 3 diffractometer	142315 measured reflections
Radiation source: fine-focus sealed tube	7105 independent reflections
Graphite monochromator	6502 reflections with $I > 2\sigma(I)$
Detector resolution: 7.3910 pixels mm^{-1}	$R_{int} = 0.052$
φ and ω scans	$\theta_{max} = 33.2°$, $\theta_{min} = 2.8°$
Absorption correction: numerical (*SADABS*; Krause *et al.*, 2015)	$h = -13 \rightarrow 13$
	$k = -22 \rightarrow 22$
	$l = -23 \rightarrow 23$
$T_{min} = 0.98$, $T_{max} = 0.98$	

Refinement

Refinement on F^2	Secondary atom site location: difference Fourier map
Least-squares matrix: full	
$R[F^2 > 2\sigma(F^2)] = 0.037$	Hydrogen site location: mixed
$wR(F^2) = 0.097$	H atoms treated by a mixture of independent and constrained refinement
$S = 1.07$	$w = 1/[\sigma^2(F_o^2) + (0.053P)^2 + 0.2332P]$ where $P = (F_o^2 + 2F_c^2)/3$
7105 reflections	
247 parameters	$(\Delta/\sigma)_{max} < 0.001$
1 restraint	$\Delta\rho_{max} = 0.29$ e Å^{-3}
Primary atom site location: dual	$\Delta\rho_{min} = -0.19$ e Å^{-3}

Absolute structure: Flack x determined using 2747 quotients $[(I^+)-(I^-)]/[(I^+)+(I^-)]$ (Parsons *et al.*, 2013)

Absolute structure parameter: 0.12 (18)

Special details

Experimental. The diffraction data were obtained from 13 sets of frames, each of width 0.5° in ω or φ, collected with scan parameters determined by the "strategy" routine in *APEX4*. The scan time was 10 sec/frame.

Geometry. All esds (except the esd in the dihedral angle between two l.s. planes) are estimated using the full covariance matrix. The cell esds are taken into account individually in the estimation of esds in distances, angles and torsion angles; correlations between esds in cell parameters are only used when they are defined by crystal symmetry. An approximate (isotropic) treatment of cell esds is used for estimating esds involving l.s. planes.

Refinement. Refinement of F^2 against ALL reflections. The weighted R-factor wR and goodness of fit S are based on F^2, conventional R-factors R are based on F, with F set to zero for negative F^2. The threshold expression of $F^2 > 2\text{sigma}(F^2)$ is used only for calculating R-factors(gt) etc. and is not relevant to the choice of reflections for refinement. R-factors based on F^2 are statistically about twice as large as those based on F, and R- factors based on ALL data will be even larger. H-atoms attached to carbon were placed in calculated positions (C—H = 0.95 - 0.99 Å) and were included as riding contributions with isotropic displacement parameters 1.2 - 1.5 times those of the attached atoms. That attached to nitrogen was placed in a location derived from a difference map and refined with a DFIX 0.91 0.01 instruction. Two reflections affected by the beamstop were omitted from the final refinement.

Fractional atomic coordinates and isotropic or equivalent isotropic displacement parameters (Å²)

	x	y	z	$U_{iso}*/U_{eq}$
O1	0.39043 (13)	0.39185 (7)	0.33591 (7)	0.0263 (2)
O2	0.66443 (13)	0.37492 (8)	0.59106 (7)	0.0278 (2)
O3	0.95278 (13)	0.37405 (8)	0.16772 (6)	0.0265 (2)
N1	0.54354 (13)	0.36178 (7)	0.45643 (7)	0.01860 (19)
N2	0.50404 (13)	0.49047 (8)	0.53375 (7)	0.01892 (19)
H2	0.518 (2)	0.5333 (12)	0.5767 (10)	0.028*
N3	0.80935 (12)	0.33366 (8)	0.33144 (7)	0.01897 (19)
C1	0.42318 (14)	0.50910 (8)	0.45190 (7)	0.01579 (19)
C2	0.44728 (14)	0.41472 (8)	0.40476 (8)	0.0177 (2)
C3	0.58023 (14)	0.40760 (9)	0.53453 (8)	0.0191 (2)
C4	0.24609 (14)	0.52644 (8)	0.46447 (8)	0.0175 (2)
C5	0.16580 (16)	0.48701 (9)	0.53445 (9)	0.0226 (2)
H5	0.222361	0.451978	0.576640	0.027*
C6	0.00231 (18)	0.49893 (10)	0.54266 (11)	0.0296 (3)
H6	−0.052435	0.471165	0.589914	0.036*
C7	−0.07996 (17)	0.55110 (12)	0.48207 (12)	0.0331 (3)
H7	−0.191083	0.559368	0.487913	0.040*
C8	−0.00078 (18)	0.59125 (11)	0.41300 (11)	0.0308 (3)
H8	−0.057409	0.627726	0.371901	0.037*
C9	0.16234 (16)	0.57833 (10)	0.40347 (9)	0.0233 (2)
H9	0.216069	0.604987	0.355331	0.028*
C10	0.50534 (14)	0.58919 (8)	0.40337 (8)	0.01677 (19)
C11	0.51864 (16)	0.67518 (9)	0.44551 (8)	0.0221 (2)
H11	0.473587	0.683179	0.501458	0.026*
C12	0.59746 (18)	0.74927 (9)	0.40608 (10)	0.0264 (3)
H12	0.607929	0.807213	0.435648	0.032*

C13	0.66094 (17)	0.73867 (10)	0.32348 (10)	0.0267 (3)
H13	0.713846	0.789458	0.296334	0.032*
C14	0.64681 (18)	0.65389 (11)	0.28097 (9)	0.0276 (3)
H14	0.689747	0.646667	0.224429	0.033*
C15	0.56972 (16)	0.57888 (10)	0.32074 (8)	0.0234 (2)
H15	0.561162	0.520695	0.291395	0.028*
C16	0.60778 (16)	0.27040 (9)	0.43367 (9)	0.0226 (2)
H16A	0.546571	0.244049	0.384678	0.027*
H16B	0.596317	0.227562	0.483704	0.027*
C17	0.78214 (15)	0.27672 (9)	0.40832 (9)	0.0211 (2)
H17A	0.842599	0.303505	0.457389	0.025*
H17B	0.823018	0.212874	0.397594	0.025*
C18	0.97742 (15)	0.35809 (9)	0.32419 (8)	0.0207 (2)
H18A	1.041537	0.300511	0.318035	0.025*
H18B	1.012307	0.391079	0.377290	0.025*
C19	1.00178 (18)	0.42037 (10)	0.24594 (9)	0.0248 (2)
H19A	0.940012	0.478672	0.253294	0.030*
H19B	1.115096	0.437442	0.241412	0.030*
C20	0.79025 (19)	0.34662 (12)	0.17402 (9)	0.0300 (3)
H20A	0.759366	0.312437	0.120832	0.036*
H20B	0.722946	0.403102	0.178463	0.036*
C21	0.76244 (18)	0.28487 (11)	0.25229 (9)	0.0275 (3)
H21A	0.648961	0.267850	0.255688	0.033*
H21B	0.824646	0.226537	0.246373	0.033*

Atomic displacement parameters (Å^2)

	U^{11}	U^{22}	U^{33}	U^{12}	U^{13}	U^{23}
O1	0.0291 (5)	0.0253 (5)	0.0245 (4)	0.0031 (4)	−0.0078 (4)	−0.0074 (4)
O2	0.0265 (5)	0.0329 (5)	0.0241 (4)	0.0036 (4)	−0.0062 (4)	0.0087 (4)
O3	0.0301 (5)	0.0309 (5)	0.0183 (4)	−0.0040 (4)	0.0023 (4)	0.0015 (4)
N1	0.0176 (4)	0.0177 (4)	0.0204 (4)	0.0023 (3)	0.0009 (4)	0.0018 (3)
N2	0.0198 (4)	0.0217 (4)	0.0153 (4)	0.0013 (4)	−0.0035 (4)	−0.0007 (3)
N3	0.0169 (4)	0.0219 (4)	0.0181 (4)	−0.0002 (4)	0.0000 (4)	0.0025 (4)
C1	0.0148 (5)	0.0178 (5)	0.0148 (4)	0.0005 (4)	−0.0015 (4)	−0.0007 (4)
C2	0.0159 (5)	0.0177 (5)	0.0193 (5)	0.0007 (4)	0.0000 (4)	−0.0009 (4)
C3	0.0158 (5)	0.0228 (5)	0.0187 (5)	−0.0012 (4)	0.0002 (4)	0.0043 (4)
C4	0.0152 (5)	0.0169 (4)	0.0202 (5)	0.0003 (4)	−0.0004 (4)	−0.0016 (4)
C5	0.0205 (5)	0.0199 (5)	0.0273 (6)	−0.0007 (4)	0.0041 (5)	0.0001 (4)
C6	0.0209 (6)	0.0281 (6)	0.0398 (8)	−0.0038 (5)	0.0087 (6)	−0.0057 (6)
C7	0.0148 (5)	0.0364 (7)	0.0480 (9)	0.0012 (5)	0.0002 (6)	−0.0126 (7)
C8	0.0211 (6)	0.0327 (7)	0.0386 (8)	0.0062 (5)	−0.0096 (6)	−0.0042 (6)
C9	0.0196 (5)	0.0252 (6)	0.0250 (5)	0.0026 (5)	−0.0048 (5)	0.0003 (5)
C10	0.0149 (4)	0.0189 (5)	0.0165 (4)	0.0008 (4)	−0.0006 (4)	0.0005 (4)
C11	0.0248 (6)	0.0200 (5)	0.0214 (5)	−0.0001 (4)	0.0027 (4)	−0.0015 (4)
C12	0.0279 (6)	0.0198 (5)	0.0315 (6)	−0.0018 (5)	0.0004 (5)	0.0020 (5)
C13	0.0214 (6)	0.0280 (6)	0.0305 (6)	−0.0008 (5)	0.0015 (5)	0.0100 (5)
C14	0.0249 (6)	0.0354 (7)	0.0225 (5)	0.0010 (5)	0.0053 (5)	0.0060 (5)

C15	0.0239 (6)	0.0274 (6)	0.0189 (5)	0.0007 (5)	0.0030 (4)	−0.0013 (4)
C16	0.0221 (6)	0.0167 (5)	0.0288 (6)	0.0022 (4)	0.0056 (5)	0.0039 (4)
C17	0.0196 (5)	0.0215 (5)	0.0223 (5)	0.0048 (4)	0.0028 (4)	0.0058 (4)
C18	0.0184 (5)	0.0246 (5)	0.0192 (5)	−0.0017 (4)	−0.0007 (4)	0.0021 (4)
C19	0.0273 (6)	0.0256 (6)	0.0214 (5)	−0.0061 (5)	0.0010 (5)	0.0020 (5)
C20	0.0290 (7)	0.0413 (8)	0.0198 (5)	−0.0061 (6)	−0.0050 (5)	0.0036 (5)
C21	0.0279 (6)	0.0321 (7)	0.0224 (6)	−0.0099 (5)	−0.0031 (5)	0.0003 (5)

Geometric parameters (Å, º)

O1—C2	1.2105 (15)	C10—C15	1.3933 (17)
O2—C3	1.2183 (15)	C10—C11	1.3955 (17)
O3—C20	1.4306 (19)	C11—C12	1.3912 (19)
O3—C19	1.4373 (17)	C11—H11	0.9500
N1—C2	1.3670 (16)	C12—C13	1.390 (2)
N1—C3	1.4058 (16)	C12—H12	0.9500
N1—C16	1.4579 (16)	C13—C14	1.383 (2)
N2—C3	1.3485 (16)	C13—H13	0.9500
N2—C1	1.4597 (15)	C14—C15	1.397 (2)
N2—H2	0.910 (12)	C14—H14	0.9500
N3—C17	1.4568 (16)	C15—H15	0.9500
N3—C21	1.4608 (17)	C16—C17	1.5260 (18)
N3—C18	1.4658 (16)	C16—H16A	0.9900
C1—C4	1.5281 (16)	C16—H16B	0.9900
C1—C10	1.5342 (16)	C17—H17A	0.9900
C1—C2	1.5465 (16)	C17—H17B	0.9900
C4—C9	1.3913 (17)	C18—C19	1.5140 (18)
C4—C5	1.3938 (17)	C18—H18A	0.9900
C5—C6	1.3967 (19)	C18—H18B	0.9900
C5—H5	0.9500	C19—H19A	0.9900
C6—C7	1.383 (2)	C19—H19B	0.9900
C6—H6	0.9500	C20—C21	1.514 (2)
C7—C8	1.383 (2)	C20—H20A	0.9900
C7—H7	0.9500	C20—H20B	0.9900
C8—C9	1.397 (2)	C21—H21A	0.9900
C8—H8	0.9500	C21—H21B	0.9900
C9—H9	0.9500		
C20—O3—C19	110.21 (11)	C13—C12—H12	119.9
C2—N1—C3	111.86 (10)	C11—C12—H12	119.9
C2—N1—C16	125.27 (11)	C14—C13—C12	119.77 (13)
C3—N1—C16	122.83 (11)	C14—C13—H13	120.1
C3—N2—C1	113.03 (10)	C12—C13—H13	120.1
C3—N2—H2	121.6 (13)	C13—C14—C15	120.34 (13)
C1—N2—H2	124.5 (13)	C13—C14—H14	119.8
C17—N3—C21	111.74 (11)	C15—C14—H14	119.8
C17—N3—C18	110.36 (10)	C10—C15—C14	120.15 (13)
C21—N3—C18	108.22 (10)	C10—C15—H15	119.9

N2—C1—C4	112.19 (9)	C14—C15—H15	119.9
N2—C1—C10	110.29 (9)	N1—C16—C17	111.56 (11)
C4—C1—C10	112.54 (10)	N1—C16—H16A	109.3
N2—C1—C2	100.70 (9)	C17—C16—H16A	109.3
C4—C1—C2	109.27 (9)	N1—C16—H16B	109.3
C10—C1—C2	111.27 (9)	C17—C16—H16B	109.3
O1—C2—N1	126.69 (12)	H16A—C16—H16B	108.0
O1—C2—C1	126.59 (11)	N3—C17—C16	113.19 (10)
N1—C2—C1	106.71 (10)	N3—C17—H17A	108.9
O2—C3—N2	128.46 (13)	C16—C17—H17A	108.9
O2—C3—N1	124.27 (12)	N3—C17—H17B	108.9
N2—C3—N1	107.27 (10)	C16—C17—H17B	108.9
C9—C4—C5	119.48 (12)	H17A—C17—H17B	107.8
C9—C4—C1	119.88 (11)	N3—C18—C19	109.42 (11)
C5—C4—C1	120.57 (11)	N3—C18—H18A	109.8
C4—C5—C6	120.11 (13)	C19—C18—H18A	109.8
C4—C5—H5	119.9	N3—C18—H18B	109.8
C6—C5—H5	119.9	C19—C18—H18B	109.8
C7—C6—C5	120.07 (14)	H18A—C18—H18B	108.2
C7—C6—H6	120.0	O3—C19—C18	111.03 (11)
C5—C6—H6	120.0	O3—C19—H19A	109.4
C8—C7—C6	120.12 (13)	C18—C19—H19A	109.4
C8—C7—H7	119.9	O3—C19—H19B	109.4
C6—C7—H7	119.9	C18—C19—H19B	109.4
C7—C8—C9	120.18 (14)	H19A—C19—H19B	108.0
C7—C8—H8	119.9	O3—C20—C21	111.28 (12)
C9—C8—H8	119.9	O3—C20—H20A	109.4
C4—C9—C8	120.03 (14)	C21—C20—H20A	109.4
C4—C9—H9	120.0	O3—C20—H20B	109.4
C8—C9—H9	120.0	C21—C20—H20B	109.4
C15—C10—C11	119.20 (11)	H20A—C20—H20B	108.0
C15—C10—C1	122.93 (11)	N3—C21—C20	110.21 (12)
C11—C10—C1	117.85 (10)	N3—C21—H21A	109.6
C12—C11—C10	120.40 (12)	C20—C21—H21A	109.6
C12—C11—H11	119.8	N3—C21—H21B	109.6
C10—C11—H11	119.8	C20—C21—H21B	109.6
C13—C12—C11	120.12 (13)	H21A—C21—H21B	108.1
C3—N2—C1—C4	122.71 (11)	C5—C4—C9—C8	0.5 (2)
C3—N2—C1—C10	−110.98 (12)	C1—C4—C9—C8	177.51 (12)
C3—N2—C1—C2	6.63 (13)	C7—C8—C9—C4	−1.2 (2)
C3—N1—C2—O1	−176.25 (13)	N2—C1—C10—C15	120.60 (12)
C16—N1—C2—O1	6.2 (2)	C4—C1—C10—C15	−113.30 (13)
C3—N1—C2—C1	3.02 (13)	C2—C1—C10—C15	9.72 (16)
C16—N1—C2—C1	−174.56 (11)	N2—C1—C10—C11	−57.84 (14)
N2—C1—C2—O1	173.71 (13)	C4—C1—C10—C11	68.27 (14)
C4—C1—C2—O1	55.47 (16)	C2—C1—C10—C11	−168.71 (11)
C10—C1—C2—O1	−69.40 (16)	C15—C10—C11—C12	−1.04 (19)

N2—C1—C2—N1	−5.56 (12)	C1—C10—C11—C12	177.46 (12)
C4—C1—C2—N1	−123.80 (10)	C10—C11—C12—C13	1.3 (2)
C10—C1—C2—N1	111.33 (11)	C11—C12—C13—C14	−0.6 (2)
C1—N2—C3—O2	175.70 (13)	C12—C13—C14—C15	−0.3 (2)
C1—N2—C3—N1	−5.21 (14)	C11—C10—C15—C14	0.14 (19)
C2—N1—C3—O2	−179.73 (12)	C1—C10—C15—C14	−178.28 (12)
C16—N1—C3—O2	−2.09 (19)	C13—C14—C15—C10	0.5 (2)
C2—N1—C3—N2	1.13 (14)	C2—N1—C16—C17	103.66 (14)
C16—N1—C3—N2	178.77 (11)	C3—N1—C16—C17	−73.66 (15)
N2—C1—C4—C9	155.69 (11)	C21—N3—C17—C16	−74.95 (14)
C10—C1—C4—C9	30.62 (15)	C18—N3—C17—C16	164.58 (11)
C2—C1—C4—C9	−93.51 (13)	N1—C16—C17—N3	−62.76 (15)
N2—C1—C4—C5	−27.35 (15)	C17—N3—C18—C19	−177.76 (11)
C10—C1—C4—C5	−152.43 (11)	C21—N3—C18—C19	59.69 (14)
C2—C1—C4—C5	83.44 (13)	C20—O3—C19—C18	57.57 (16)
C9—C4—C5—C6	0.58 (19)	N3—C18—C19—O3	−59.72 (15)
C1—C4—C5—C6	−176.39 (12)	C19—O3—C20—C21	−56.62 (17)
C4—C5—C6—C7	−1.0 (2)	C17—N3—C21—C20	179.21 (12)
C5—C6—C7—C8	0.3 (2)	C18—N3—C21—C20	−59.08 (15)
C6—C7—C8—C9	0.8 (2)	O3—C20—C21—N3	58.29 (17)

Hydrogen-bond geometry (Å, º)

Cg3 is the centroid of the C4–C9 benzene ring.

D—H···A	D—H	H···A	D···A	D—H···A
N2—H2···O3[i]	0.91 (1)	1.95 (1)	2.8560 (15)	179 (2)
C12—H12···Cg3[ii]	0.95	2.62	3.5576 (15)	169
C18—H18B···Cg3[iii]	0.99	2.65	3.5726 (14)	155

Symmetry codes: (i) −x+3/2, −y+1, z+1/2; (ii) −x, y+3/2, −z+3/2; (iii) x+1, y, z.